

Global Rotation of Skyrmion Bags under Vertical Microwave Fields

Lan Bo,^{1,2} Rongzhi Zhao,^{3, a)} Xichao Zhang,¹ Masahito Mochizuki,^{1, b)} and Xuefeng Zhang^{2,3}

¹⁾*Department of Applied Physics, Waseda University, Okubo, Shinjuku-ku, Tokyo 169-8555,*

Japan

²⁾*Key Laboratory for Anisotropy and Texture of Materials (MOE), School of Materials Science and Engineering, Northeastern University, Shenyang 110819, China*

³⁾*Institute of Advanced Magnetic Materials, College of Materials and Environmental Engineering, Hangzhou Dianzi University, Hangzhou 310012, China*

(Dated: 26 February 2024)

Magnetic skyrmion bags are composite topological spin textures with arbitrary topological charges. Here, we computationally study the transient rotational motion of skyrmion bags, which is characterized by a global rotation of the inner skyrmions around the central point. Distinct from conventional rotational modes found in skyrmions, the observed rotation is a forced motion associated with the breathing mode induced solely by vertical microwave fields. The driving force behind this rotation originates from the interactions between outer and inner skyrmions, with the angular velocity determined by the phase difference resulting from their asynchronous breathing behaviors. It is also found that skyrmion bags with larger skyrmion numbers are more conducive to the occurrence of the rotation. Our results are useful for understanding the cluster dynamics of complex topological spin textures driven by dynamic fields.

I. INTRODUCTION

Magnetic skyrmions are topologically nontrivial spin textures and have garnered substantial attention and interest in various of fields ranging from fundamental physics to materials science.^{1–8} Notably, recent advances in the exploration of localized spin configurations lead to the expansion of the skyrmion family.^{9–15} For example, elementary particle-like skyrmions may be assembled together to form composite structures known as skyrmion bags,¹⁶ which consist of an outer skyrmion boundary (i.e., a circular domain wall) enveloping multiple smaller nested skyrmions. Skyrmion bags were initially proposed in 2019,^{16,17} and have since been experimentally detected in diverse materials, such as B20-type chiral magnets¹⁸ and van der Waals magnets.¹⁹ They have also been verified as transition states in the transformation processes involving skyrmions and skyrmioniums,²⁰ as well as in the generation of skyrmion-antiskyrmion pairs.²¹ The arbitrary topological charges endow skyrmion bags with the potential to enable high-density and multi-data information encoding,^{16,17} thereby attracting extensive theoretical investigations, including their existence and stability,²² controllable creation,²³ and dynamics driven by spin-orbit torques,²⁴ spin-transfer torques,²⁵ anisotropy gradient,²⁶ and voltage gates.^{27,28} Moreover, skyrmion bags could also serve as compelling evidence to physically explicate the particle-continuum duality²⁹ and extraordinary diversity³⁰ of the skyrmion solutions. Therefore, the study of skyrmion bags is of academic significance and may lead to practical applications.

The spin excitation of topological spin textures under microwave fields is an important issue in the control and manipulation of their dynamics. Dynamic responses in both skyrmion crystals^{31,32} and individual skyrmion

have been investigated, where three eigenmodes have been identified. Specifically, these modes include a breathing mode under out-of-plane microwave fields, as well as clockwise and anticlockwise rotational modes under in-plane microwave fields.^{31–34} These resonance effects suggest an opportunity for the design and development of skyrmion-based microwave applications including microwave detectors^{35,36} and nano-oscillators.^{37,38} Furthermore, subsequent works have extended to other skyrmionic textures, such as antiskyrmion,^{39,40} skyrmionium,⁴¹ bimeron,⁴² and hopfion,^{43,44} whose individual spin eigenmodes can serve as unique fingerprints to enable their differentiation.⁴⁵

The spin excitation of skyrmion bags under out-of-plane⁴⁶ and in-plane microwave fields⁴⁷ have been explored very recently, with various oscillation modes identified. These works involved skyrmion bags with small skyrmion numbers and high central symmetry, constrained within a nanodisk. In this paper, we find that a global rotation of the skyrmion bags can be driven by a microwave field, where skyrmion bags with notably large skyrmion number is considered in an open boundary framework. The initial skyrmion bags inherently adopt a hexagonal spatial arrangement similar to the skyrmion crystals.⁴⁸ Different from the conventional skyrmion rotational modes induced by in-plane microwave fields^{31–34}, the observed transient rotation is believed to be a forced motion affiliated to the high-frequency response mode purely triggered by vertical microwave fields.

II. MODEL AND METHODOLOGY

As illustrated schematically in Fig. 1 (a), the model considered in this work is a two-dimensional (2D) square lattice consisting of $N = 250 \times 250$ sites, designed to simulate a magnetic thin film. A skyrmion bag with skyrmion number $|Q| = 18$ is set as the initial spin configuration after full

^{a)}Corresponding E-mail: zhaorz@hdu.edu.cn

^{b)}Corresponding E-mail: masa_mochizuki@waseda.jp

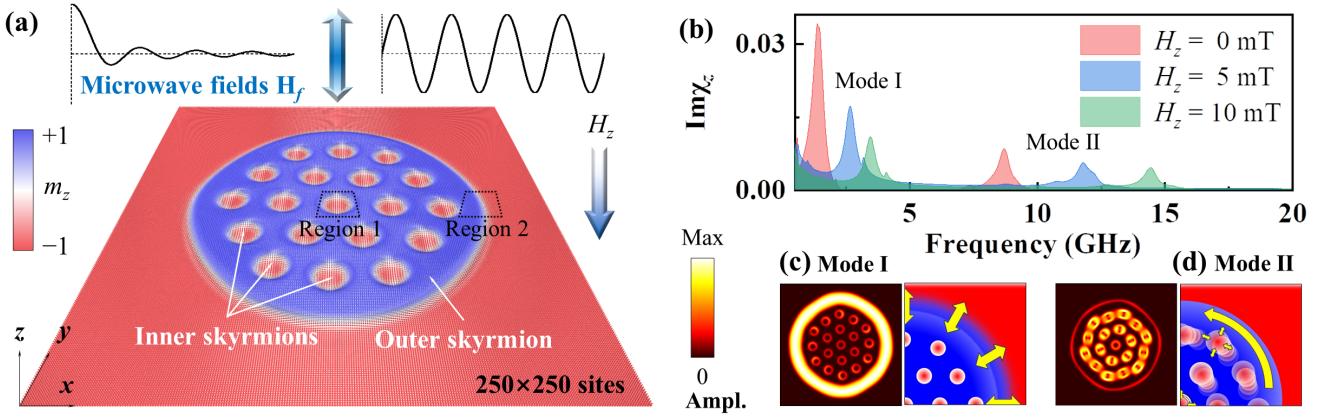


FIG. 1. (a) Schematic of the micromagnetic model: a 2D magnetic film comprising a grid of 250×250 sites. The initial skyrmion bag consists of an outer skyrmion and nineteen inner skyrmions with opposite polarity. Regions 1 and 2 are squared areas each spanning dimensions of 30×30 sites, located at the central or along the border areas of the skyrmion bags, respectively. A uniform external field $-H_z$ is applied across the entire space. Microwave magnetic fields with sinc-function and sin-function profiles are shown as insets. The color bar of magnetization component m_z is also applicable to all subsequent spin configurations. (b) Imaginary part of the susceptibility spectrum obtained after applying a sinc-function field. Two resonance peaks under $H_z = 0$ are located at $f_I = 1.4$ GHz and $f_{II} = 8.7$. Insets: schematic illustrations of the dynamic changes for the two spin excitation modes. (c) (d) The spatial FFT amplitude distributions of the z-component magnetization m_z . The color bar indicates the intensity of the oscillation amplitude.

relaxation.²³ Here, the skyrmion number is defined as¹

$$Q = \frac{1}{4\pi} \int \mathbf{m} \cdot (\partial_x \mathbf{m} \times \partial_y \mathbf{m}) dx dy, \quad (1)$$

where \mathbf{m} is the normalized magnetization vector, and $n = |Q| + 1$ is the actual number of the inner skyrmions because that the outer skyrmion carries $Q = 1$. The diameter of the outer skyrmion is around 180 sites, which avoids the potential influence of finite geometric constraints. The average energy density of this system is given by

$$\begin{aligned} \varepsilon = & A(\nabla \mathbf{m})^2 + D[m_z(\nabla \cdot \mathbf{m}) - (\mathbf{m} \cdot \nabla)m_z] \\ & - K(\mathbf{n} \cdot \mathbf{m})^2 - \mu_0 M_s m_z H_z - \frac{1}{2} \mu_0 M_s \mathbf{m} \cdot \mathbf{H}_{\text{dm}}, \end{aligned} \quad (2)$$

where A , D , and K are the Heisenberg exchange, interfacial Dzyaloshinskii-Moriya interaction (DMI), and perpendicular anisotropy constants, respectively. The vector \mathbf{n} is the unit surface normal vector, μ_0 is the vacuum permeability, M_s is the saturation magnetization, H_z is the strength of the static applied magnetic field along the $-z$ direction, and \mathbf{H}_{dm} is the demagnetizing field. To describe the dynamic behaviors of the skyrmion bags, we employ the finite-difference micromagnetic solver MUMAX3,⁴⁹ for the integration of the Landau-Lifshitz-Gilbert equation

$$\partial_t \mathbf{m} = -\gamma_0 \mathbf{m} \times \mathbf{h}_{\text{eff}} + \alpha (\mathbf{m} \times \partial_t \mathbf{m}), \quad (3)$$

where γ_0 is the absolute gyromagnetic ratio, α is the Gilbert damping constant, and $\mathbf{h}_{\text{eff}} = -(\delta \varepsilon / \delta \mathbf{m}) / (\mu_0 M_s)$ is the effective field. The key input parameters are derived from Co/Pt films in real experiments^{50,51} and some previous theoretical works:²²⁻²⁴ $M_s = 5.8 \times 10^5$ A/m, $A = 1.5 \times 10^{-11}$ J/m, $D = 3.5 \times 10^{-3}$ J/m², $K = 8.0 \times 10^5$ J/m³, and $\alpha = 0.01 - 0.05$ depending on various situations.

III. RESULTS AND DISCUSSION

Our investigation starts by identifying the spin excitation modes of the skyrmion bags under vertical microwave fields. We apply an alternating current (AC) magnetic field $\mathbf{H}_f = [0, 0, H_0^* \sin(2\pi f t) / (2\pi f t)]$, with the amplitude $H_0^* = 1$ mT and the cutoff frequency $f = 50$ GHz, and its profile can be found in the inset of Fig. 1 (a). The spin excitation spectra under different H_z are given in Fig. 1 (b), where the imaginary part of the dynamical susceptibility, $\text{Im}\chi_z$, is calculated from the fast Fourier transformation (FFT) of magnetization component $m_z(t) = (1/N) \sum_{i=1}^N m_{z,i}(t)$. Note that we present only the range within 20 GHz since there are no apparent resonance peaks observed beyond this range. Two notable resonance peaks have been identified, and these peaks exhibit a shift towards higher frequency intervals with the increase of H_z , while simultaneously weakening in strength. To further trace the spin dynamics of each mode, we consider the case where $H_z = 0$ and apply sin-function AC fields $\mathbf{H}_f = [0, 0, H_0 \sin(2\pi f_i t)]$, with the amplitude $H_0 = 15$ mT and two eigenfrequencies $f_I = 1.4$ GHz, $f_{II} = 8.7$ GHz. The profile of such microwave fields is also shown in the inset of Fig. 1 (a). Figures 1 (c) (d) depict the amplitude distributions of the oscillation obtained through FFT for each spatial point. It is revealed that mode I primarily corresponds to the breathing mode of the outer skyrmion, whereas mode II is mainly the breathing mode of the inner skyrmions, accompanied by a collective rotational motion. The corresponding schematic illustrations of the spin dynamics for each mode are also shown at the side in Fig. 1 (c) (d). Interestingly, in previous studies concerning skyrmion excitations,³¹⁻³³ there have been no instances where a vertical magnetic field induced a rotational mode. So our following investigation will focus on characterizing and analyzing this rotational motion.

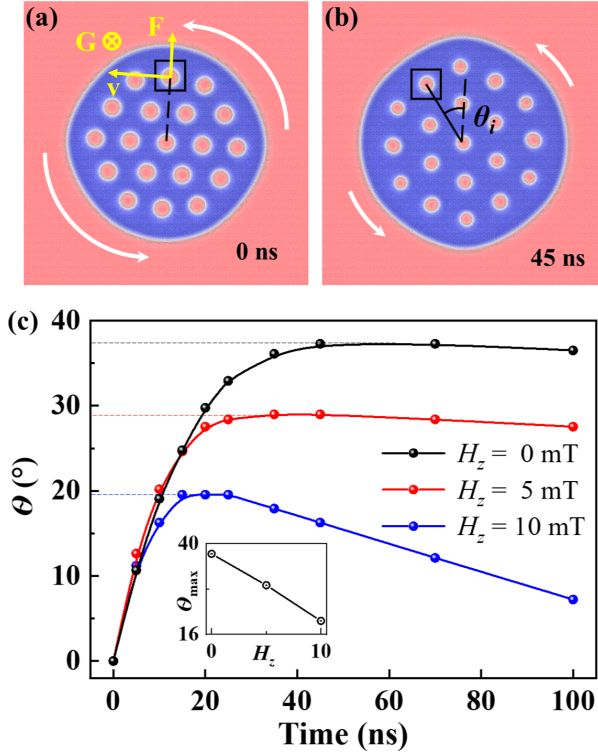


FIG. 2. Selected snapshots of dynamic spin textures for a microwave-irradiated skyrmion bag with rotating inner skyrmions at (a) $t = 0$ ns, and (b) $t = 45$ ns. The rotational direction is indicated by white arrows. The schematic of Magnus force is indicated by yellow arrows. θ_i is the rotation angle of an inner skyrmion. (c) Time profiles of the rotation angle Θ for various H_z . Inset: Variation of the maximum value of the rotation angle Θ_{max} versus H_z .

Now we undertake the characterization of the rotational dynamics of the skyrmion bags. Figure 2 (a) (b) present the snapshots of the dynamic spin configurations throughout the rotation process under $H_z = 0$. It is evident that the inner skyrmions collectively engage in an anticlockwise rotation around the central point. We trace a marked inner skyrmion as an example, which, at a given moment t , will rotate by an angle denoted as $\theta_i(t)$, from its initial position. Here, i is the index of inner skyrmions. As shown in the inset of Fig. 2 (a), because the shape of inner skyrmions remain unchanged, the direction of rotation can be determined by the Thiele framework⁵² $\mathbf{G} \times \mathbf{v} \sim \mathbf{F}$, where $\mathbf{G} = (0, 0, 4\pi Q)$ is the gyromagnetic coupling vector, \mathbf{v} is the skyrmion velocity, and \mathbf{F} is the interaction force from the outer skyrmion boundary. This equation indicates that the moving direction of skyrmion ($\|\mathbf{v} \propto \mathbf{F} \times \mathbf{G}\|$) is perpendicular to \mathbf{F} . More specifically, because the inner skyrmions have $Q = -1$, the force from the outer skyrmion boundary drives their motion in the azimuth direction of anticlockwise (clockwise) sense, when \mathbf{F} is attractive (repulsive). Then, we introduce the rotation angle of the skyrmion bags $\Theta(t) = (1/n) \sum_{i=1}^n \theta_i(t)$, with $\theta_i(t)$ being the rotation angle of each inner skyrmion. The variation of Θ versus time under different H_z is shown in Fig. 2 (c). It can be seen that the rotational motion is a transient phenomenon. Specifi-

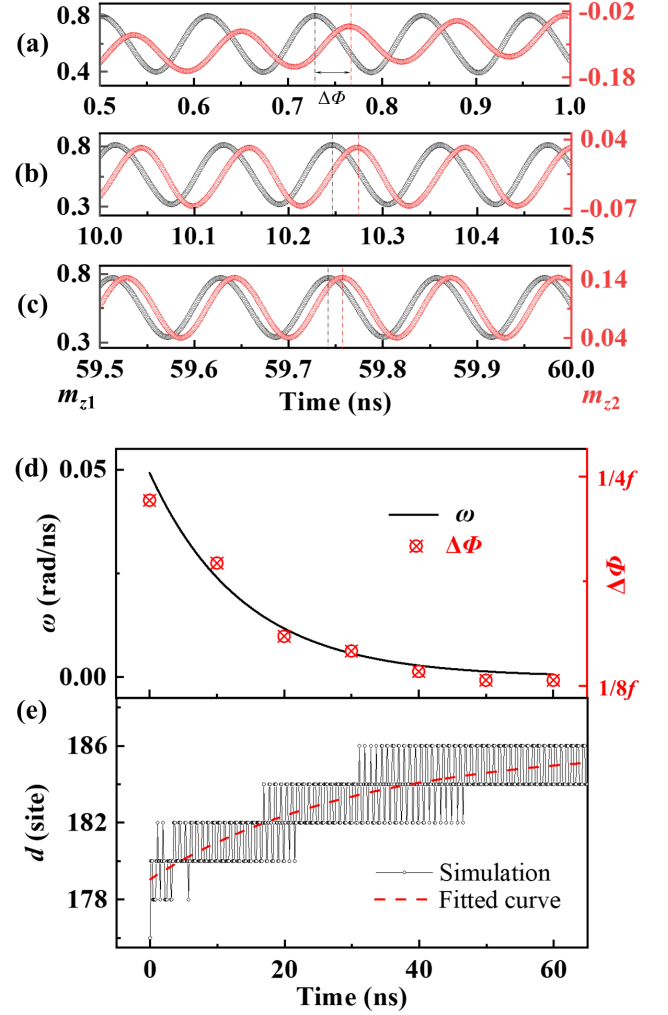


FIG. 3. Variations of the z -component magnetizations in Region 1 and 2, m_{z1} and m_{z2} , plotted as a function of time within 0.5 ns, for three distinct intervals: (a) Initial stage spanning from 0.5 ns to 1.0 ns; (b) Intermediate stage spanning from 10.0 ns to 10.5 ns; (c) Stable stage spanning from 59.5 ns to 60.0 ns. $\Delta\Phi$ represents the phase difference between $m_{z1}(t)$ and $m_{z2}(t)$. (d) Time-dependent variations of the angular velocity ω (black curve) and the phase difference $\Delta\Phi$ (red data points). (e) Variation of the outer skyrmion diameter d versus time. The black line with markers represents the simulated results, while the red dashed line corresponds to the fitted curve.

cally, as time progresses, Θ exhibits a rapid increase, followed by a gradual decline. For $H_z = 0$, the maximum value of the rotation angle Θ_{max} reaches up to about 40 degrees. As H_z increases, Θ tends to reach the maximum value at an earlier stage, and Θ_{max} undergoes a gradual reduction, as shown in the inset of Fig. 2 (c). We also find that the applied static field H_z enhances the decay in Θ . This is due to the fact that as H_z increases, the outer skyrmion tends to shrink, and the inner skyrmions are subject to a repulsive force toward the center, leading to rotation in the opposite direction. The magnitude of the decay in Θ is minimal when $H_z = 0$, even as time extends to 100 ns. So the case of zero static field is exclusively

considered in the following studies.

We next aim at analyzing the physical origin of the rotational motion. As shown in Fig. 1, two distinct regions are defined in the 2D space, each with 30×30 sites. Region 1 completely covers the central inner skyrmion, and Region 2 covers part of the boundary of the outer skyrmion. The time-dependent variations of z -component magnetizations within the two regions (defined as m_{z1} and m_{z2}) are extracted, which respectively reflect the breathing behaviors of inner and outer skyrmions in response to the vertical microwave fields. We choose three representative time intervals: the initial stage from 0.5 to 1.0 ns, the intermediate stage from 10.0 to 10.5 ns, and the stable stage from 59.5 to 60.0 ns. Here, we concentrate on the time frame within 60 ns. This decision is based on the observation from Fig. 2, which indicates that the rotation angle reaches its maximum at around 45 ns, suggesting that a 60 ns window is sufficient for our analysis. In Fig. 3 (a)-(c), the variations of m_{z1} and m_{z2} are plotted as a function of time for these selected stages. Figure 3 (a) shows distinct asynchronous oscillations, where the amplitude of the oscillation curve for m_{z1} consistently remains stable, while the amplitude of m_{z2} appears weaker and unstable. We define the phase difference $\Delta\Phi$ as the time difference between the moments at which the fluctuations of m_{z1} and m_{z2} reach their peaks within one function period. It is obvious that $\Delta\Phi$ becomes smaller as time increases. At this point, we put forward a conjecture that the transient rotational motion of skyrmion bags results from the asynchrony in the breathing behaviors between the inner skyrmions and the outer skyrmion.

To verify the above hypothesis, we calculate the angular velocity ω of the rotation, which is the derivative of the rotation angle with respect to time, defined as $\omega = d\Theta/dt$. We then compare the time profile of ω with that of the phase difference $\Delta\Phi(t)$, as shown in Fig. 3 (d). From the consistency of the curve and the scatter points, we can find a significant positive correlation between ω and $\Delta\Phi$, which both decrease from an initial value and gradually stabilize. This corroborates the conclusion that the rotation is induced by the asynchrony in breathing behaviors, and further demonstrates that the velocity of the rotational motion is determined by $\Delta\Phi$. In order to investigate the underlying mechanism of the phase difference, we extracted the diameter of the outer skyrmion d as a function of time during the rotation, as shown in Fig. 3 (e). The simulation results reveal that d gradually increases during the oscillation and converge to a constant. This increasing trend is fitted by an exponential function with horizontal asymptote $d = a - b * e^c$, where $a = 186.0$, $b = 6.88$ and $c = 0.97$. Regarding this phenomenon, we offer the following explanation: in this response mode, the breathing of inner skyrmions is spontaneous, while the breathing of the outer skyrmion is induced by the former. Hence, as time progresses, the phases of their oscillations trend to gradually converge. Furthermore, when inner skyrmions start continuous breathing from the initial static state, they exert an interaction potential that encourages expansion on the passively oscillating outer skyrmion, resulting in a slight increase in d . Consequently, the reaction of this potential becomes the driving force for the forced rotation of skyrmion bags.

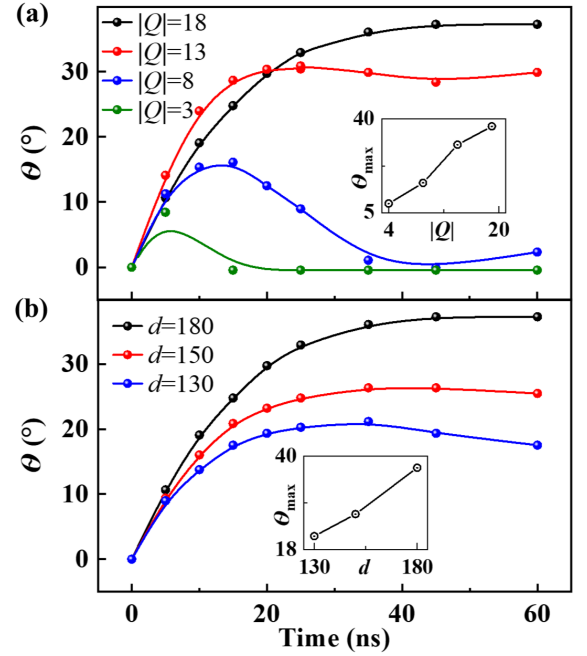


FIG. 4. (a) The rotation angle Θ plotted as a function of time for various skyrmion numbers Q . Inset: the maximum value of rotation angle Θ_{max} for the four different Q . (b) The rotation angle Θ plotted as a function of time for various outer skyrmion diameter d . Inset: the maximum value of rotation angle Θ_{max} for the three different d .

Finally, we discuss the rotation behavior of skyrmion bags with different skyrmion numbers, where $|Q| = 13, 8,$ and 3 are selected for comparison. After applying \mathbf{H}_f^* to find their resonance frequencies, we excite their high-frequency mode separately and record the time-dependent variations of Θ , as shown in Fig. 4 (a). Clearly, the variations can be categorized into two distinct trends. For skyrmion bags with $|Q| = 18$ and 13 , Θ exhibits a slight decrease or fluctuation after reaching its maximum, depending on the specific symmetry of the spin configurations; whereas for skyrmion bags with $|Q| = 8$ and 3 , Θ rapidly returns to zero after reaching its maximum, indicating a reverse rotation back to the initial position. We further extract the maximum value of rotation angle Θ_{max} , for the four situations, as shown in the inset of Fig. 4 (a). It can be summarized that for a smaller $|Q|$ of skyrmion bags, the achievable Θ_{max} tends to be smaller. This is because when there are more inner skyrmions, the overall oscillation generated by their breathing mode is stronger, resulting in a larger driving force to maintain the rotation. The results indicate that the rotation is more likely to occur for skyrmion bags with larger $|Q|$, while it is less likely to be observed in skyrmion bags with smaller $|Q|$. Interestingly, we noticed that as $|Q|$ decreases, the diameter of the outer skyrmion d also decreases at the same time. In order to verify whether the above conclusion is attributed by changes in $|Q|$ or d , we conducted additional simulations by proportionally reducing d through adjusting the DMI constant. The impact of d on the rotational behavior is illustrated in Fig. 4 (b). The reduction of d does weaken the rotation, indicating that, for a constant $|Q|$, the rotational

behavior is more pronounced in larger-sized skyrmion bags. However, the decrease in d does not lead to a rapid decay similar to that observed for smaller $|Q|$. Because d is approximately 130 sites when $|Q| = 8$, we can compare the results of $|Q| = 8$ and $d = 130$ to confirm this point.

IV. CONCLUSION AND PROSPECT

In conclusion, we have investigated a global rotational motion of skyrmion bags in response to microwave magnetic fields. This behavior is specific to the high-frequency mode, and is characterized by the inner skyrmions rotating cohesively around the central point. It has been proven that the angular velocity of the rotation is directly related to the phase difference between the oscillations of inner and outer skyrmions. And the driving force of the rotation arises from the interaction potential of the outer skyrmion boundary acting on the inner skyrmions. It is also found that the rotation is more prone to occur in skyrmion bags with larger skyrmion numbers.

Although the rotation is a transient dynamics, it enables the possibility of manipulation of skyrmion bags by activating the eigenmode. Specially, it induces both spatial and temporal variations in magnetization, providing potential to generate rich spintronic phenomena and applications such as spinmotive force⁴⁸ and programmable logic device.⁵³ In a real system, the rotation may be influenced by temperature, but we believe that under small thermal fluctuations, the skyrmion bag will experience some distortion without undergoing fundamental changes in its rotational behavior.⁴⁸ Our findings hold significance for the microwave-controlled dynamics of skyrmion bags, and may extend to other topological configurations featuring multiple domains.

ACKNOWLEDGMENTS

X.C.Z. and M.M. acknowledge support by the JST CREST (Project No. JPMJCR20T1), the JSPS KAKENHI (Grants No. JP20H00337 and No. JP23H04522), and the Waseda University Grant for Special Research Projects (Grant No. 2023C-140). R.Z.Z and X.F.Z. acknowledge support by the National Science Fund for Distinguished Young Scholars (Grant No. 52225312), the National Natural Science Foundation of China (Grant No. U1908220), and the Key Research and Development Program of Zhejiang Province (Grant No. 2021C01033). L.B. thanks the financial support by China Scholarship Council (Award No. 202206080023).

AUTHOR DECLARATIONS

The authors have no conflicts to disclose.

DATA AVAILABILITY STATEMENT

The data that support the findings of this study are available from the corresponding authors upon reasonable request.

- ¹N. Nagaosa and Y. Tokura, "Topological properties and dynamics of magnetic skyrmions," *Nature nanotechnology* **8**, 899–911 (2013).
- ²M. Mochizuki and S. Seki, "Dynamical magnetoelectric phenomena of multiferroic skyrmions," *Journal of Physics: Condensed Matter* **27**, 503001 (2015).
- ³A. Fert, N. Reyren, and V. Cros, "Magnetic skyrmions: advances in physics and potential applications," *Nature Reviews Materials* **2**, 1–15 (2017).
- ⁴J. Leliaert, M. Dvornik, J. Mulkers, J. De Clercq, M. Milošević, and B. Van Waeyenberge, "Fast micromagnetic simulations on gpu—recent advances made with," *Journal of Physics D: Applied Physics* **51**, 123002 (2018).
- ⁵X. Zhang, Y. Zhou, K. M. Song, T.-E. Park, J. Xia, M. Ezawa, X. Liu, W. Zhao, G. Zhao, and S. Woo, "Skyrmion-electronics: writing, deleting, reading and processing magnetic skyrmions toward spintronic applications," *Journal of Physics: Condensed Matter* **32**, 143001 (2020).
- ⁶B. Göbel, I. Mertig, and O. A. Tretiakov, "Beyond skyrmions: Review and perspectives of alternative magnetic quasiparticles," *Physics Reports* **895**, 1–28 (2021).
- ⁷L. Bo, C. Hu, R. Zhao, and X. Zhang, "Micromagnetic manipulation and spin excitation of skyrmionic structures," *Journal of Physics D: Applied Physics* (2022).
- ⁸C. Reichhardt, C. J. O. Reichhardt, and M. Milošević, "Statics and dynamics of skyrmions interacting with disorder and nanostructures," *Reviews of Modern Physics* **94**, 035005 (2022).
- ⁹U. K. Roessler, A. Bogdanov, and C. Pfleiderer, "Spontaneous skyrmion ground states in magnetic metals," *Nature* **442**, 797–801 (2006).
- ¹⁰G. Finocchio, F. Büttner, R. Tomasello, M. Carpentieri, and M. Kläui, "Magnetic skyrmions: from fundamental to applications," *Journal of Physics D: Applied Physics* **49**, 423001 (2016).
- ¹¹W. Jiang, G. Chen, K. Liu, J. Zang, S. G. Te Velthuis, and A. Hoffmann, "Skyrmions in magnetic multilayers," *Physics Reports* **704**, 1–49 (2017).
- ¹²N. Kanazawa, S. Seki, and Y. Tokura, "Noncentrosymmetric magnets hosting magnetic skyrmions," *Advanced Materials* **29**, 1603227 (2017).
- ¹³K. Everschor-Sitte, J. Masell, R. M. Reeve, and M. Kläui, "Perspective: Magnetic skyrmions—overview of recent progress in an active research field," *Journal of Applied Physics* **124** (2018).
- ¹⁴C. Back, V. Cros, H. Ebert, K. Everschor-Sitte, A. Fert, M. Garst, T. Ma, S. Mankovsky, T. Monchesky, M. Mostovoy, *et al.*, "The 2020 skyrmionics roadmap," *Journal of Physics D: Applied Physics* **53**, 363001 (2020).
- ¹⁵Y. Fujishiro, N. Kanazawa, and Y. Tokura, "Engineering skyrmions and emergent monopoles in topological spin crystals," *Applied Physics Letters* **116** (2020).
- ¹⁶D. Foster, C. Kind, P. J. Ackerman, J.-S. B. Tai, M. R. Dennis, and I. I. Smalyukh, "Two-dimensional skyrmion bags in liquid crystals and ferromagnets," *Nature Physics* **15**, 655–659 (2019).
- ¹⁷F. N. Rybakov and N. S. Kiselev, "Chiral magnetic skyrmions with arbitrary topological charge," *Physical Review B* **99**, 064437 (2019).
- ¹⁸J. Tang, Y. Wu, W. Wang, L. Kong, B. Lv, W. Wei, J. Zang, M. Tian, and H. Du, "Magnetic skyrmion bundles and their current-driven dynamics," *Nature Nanotechnology* **16**, 1086–1091 (2021).
- ¹⁹L. Powalla, M. T. Birch, K. Litzius, S. Wintz, F. S. Yasin, L. A. Turnbull, F. Schulz, D. A. Mayoh, G. Balakrishnan, M. Weigand, *et al.*, "Seeding and emergence of composite skyrmions in a van der waals magnet," *Advanced Materials* **35**, 2208930 (2023).
- ²⁰S. Yang, Y. Zhao, K. Wu, Z. Chu, X. Xu, X. Li, J. Åkerman, and Y. Zhou, "Reversible conversion between skyrmions and skyrmioniums," *Nature Communications* **14**, 3406 (2023).
- ²¹F. Zheng, N. S. Kiselev, L. Yang, V. M. Kuchkin, F. N. Rybakov, S. Blügel, and R. E. Dunin-Borkowski, "Skyrmion–antiskyrmion pair creation and annihilation in a cubic chiral magnet," *Nature Physics* **18**, 863–868 (2022).
- ²²C. Kind, S. Friedemann, and D. Read, "Existence and stability of skyrmion bags in thin magnetic films," *Applied Physics Letters* **116**, 022413 (2020).
- ²³L. Bo, R. Zhao, C. Hu, X. Zhang, X. Zhang, and M. Mochizuki, "Controllable creation of skyrmion bags in a ferromagnetic nanodisk," *Physical Review B* **107**, 224431 (2023).

- ²⁴Z. Zeng, C. Zhang, C. Jin, J. Wang, C. Song, Y. Ma, Q. Liu, and J. Wang, “Dynamics of skyrmion bags driven by the spin-orbit torque,” *Applied Physics Letters* **117**, 172404 (2020).
- ²⁵C. Kind and D. Foster, “Magnetic skyrmion binning,” *Physical Review B* **103**, L100413 (2021).
- ²⁶Z. Zeng, N. Mehmood, Y. Ma, J. Wang, J. Wang, and Q. Liu, “The skyrmion bags in an anisotropy gradient,” *Journal of Physics: Condensed Matter* **34**, 395801 (2022).
- ²⁷R. Chen and Y. Li, “Voltage-controlled skyrmionic interconnect with multiple magnetic information carriers,” *ACS Applied Materials & Interfaces* **14**, 30420–30434 (2022).
- ²⁸Z. Zhang, M. Xu, G. Jiang, J. Zhang, D. Meng, W. Chen, Y. Chen, and C. Hu, “High-density racetrack memory based on magnetic skyrmion bags controlled by voltage gates,” *Journal of Applied Physics* **132** (2022).
- ²⁹X. Wang and X. Hu, “Particle-continuum duality of skyrmions,” *Physical Review B* **107**, 174412 (2023).
- ³⁰V. M. Kuchkin, B. Barton-Singer, F. N. Rybakov, S. Blügel, B. J. Schroers, and N. S. Kiselev, “Magnetic skyrmions, chiral kinks, and holomorphic functions,” *Physical Review B* **102**, 144422 (2020).
- ³¹M. Mochizuki, “Spin-wave modes and their intense excitation effects in skyrmion crystals,” *Physical Review Letters* **108**, 017601 (2012).
- ³²Y. Onose, Y. Okamura, S. Seki, S. Ishiwata, and Y. Tokura, “Observation of magnetic excitations of skyrmion crystal in a helimagnetic insulator Cu_2OSeO_3 ,” *Physical review letters* **109**, 037603 (2012).
- ³³J.-V. Kim, F. Garcia-Sanchez, J. Sampaio, C. Moreau-Luchaire, V. Cros, and A. Fert, “Breathing modes of confined skyrmions in ultrathin magnetic dots,” *Physical Review B* **90**, 064410 (2014).
- ³⁴Y. Liu, R. K. Lake, and J. Zang, “Shape dependent resonant modes of skyrmions in magnetic nanodisks,” *Journal of Magnetism and Magnetic Materials* **455**, 9–13 (2018).
- ³⁵M. Mochizuki and S. Seki, “Magnetolectric resonances and predicted microwave diode effect of the skyrmion crystal in a multiferroic chiral-lattice magnet,” *Physical Review B* **87**, 134403 (2013).
- ³⁶G. Finocchio, M. Ricci, R. Tomasello, A. Giordano, M. Lanuzza, V. Puliafito, P. Burrascano, B. Azzerboni, and M. Carpentieri, “Skyrmion based microwave detectors and harvesting,” *Applied Physics Letters* **107** (2015).
- ³⁷R. Liu, W. Lim, S. Urazhdin, *et al.*, “Dynamical skyrmion state in a spin current nano-oscillator with perpendicular magnetic anisotropy,” *Physical review letters* **114**, 137201 (2015).
- ³⁸C. Navau, N. Del-Valle, and A. Sanchez, “Analytical trajectories of skyrmions in confined geometries: Skyrmionic racetracks and nano-oscillators,” *Physical Review B* **94**, 184104 (2016).
- ³⁹A. Raeliarijaona, R. Nepal, and A. A. Kovalev, “Boundary twists, instabilities, and creation of skyrmions and antiskyrmions,” *Physical Review Materials* **2**, 124401 (2018).
- ⁴⁰B. McKeever, D. Rodrigues, D. Pinna, A. Abanov, J. Sinova, and K. Everschor-Sitte, “Characterizing breathing dynamics of magnetic skyrmions and antiskyrmions within the hamiltonian formalism,” *Physical Review B* **99**, 054430 (2019).
- ⁴¹H. Vigo-Cotrina, “Spin wave modes of skyrmioniums in the presence of dzyaloshinskii-moriya interaction,” *Journal of Magnetism and Magnetic Materials* **537**, 168166 (2021).
- ⁴²J. Wang, C. Zhang, Y. Ma, Z. Zeng, N. Mehmood, Y. Yuan, J. Yang, C. Song, J. Wang, and Q. Liu, “Field-dependent shape and magnetic spectrum of magnetic bimeron,” *Journal of Magnetism and Magnetic Materials* **555**, 169343 (2022).
- ⁴³Y. Liu, R. K. Lake, and J. Zang, “Binding a hopfion in a chiral magnet nanodisk,” *Physical Review B* **98**, 174437 (2018).
- ⁴⁴L. Bo, L. Ji, C. Hu, R. Zhao, Y. Li, J. Zhang, and X. Zhang, “Spin excitation spectrum of a magnetic hopfion,” *Applied Physics Letters* **119** (2021).
- ⁴⁵M. Lonsky and A. Hoffmann, “Dynamic excitations of chiral magnetic textures,” *APL Materials* **8** (2020).
- ⁴⁶Z. Zeng, C. Song, J. Wang, and Q. Liu, “Spin eigenmodes of skyrmion bags,” *Journal of Physics D: Applied Physics* **55**, 185001 (2022).
- ⁴⁷S. Li, K. Li, Z. Liu, Q. Zhu, C. Zhao, H. Zhang, X. Shi, J. Wang, R. Wang, R. Lian, *et al.*, “In-plane spin excitation of skyrmion bags,” *Chinese Physics B* (2023).
- ⁴⁸J. Matsuki and M. Mochizuki, “Thermoelectric effect of a skyrmion crystal confined in a magnetic disk,” *Physical Review B* **107**, L100408 (2023).
- ⁴⁹A. Vansteenkiste, J. Leliaert, M. Dvornik, M. Helsen, F. Garcia-Sanchez, and B. Van Waeyenberge, “The design and verification of mumax3,” *AIP advances* **4**, 107133 (2014).
- ⁵⁰J. Sampaio, V. Cros, S. Rohart, A. Thiaville, and A. Fert, “Nucleation, stability and current-induced motion of isolated magnetic skyrmions in nanostructures,” *Nature nanotechnology* **8**, 839–844 (2013).
- ⁵¹P. Metaxas, J. Jamet, A. Mougin, M. Cormier, J. Ferré, V. Baltz, B. Rodmacq, B. Dieny, and R. Stamps, “Creep and flow regimes of magnetic domain-wall motion in ultrathin $\text{Pt}/\text{Co}/\text{Pt}$ films with perpendicular anisotropy,” *Physical review letters* **99**, 217208 (2007).
- ⁵²W. Jiang, X. Zhang, G. Yu, W. Zhang, X. Wang, M. Benjamin Jungfleisch, J. E. Pearson, X. Cheng, O. Heinonen, K. L. Wang, *et al.*, “Direct observation of the skyrmion hall effect,” *Nature Physics* **13**, 162–169 (2017).
- ⁵³Z. Yan, Y. Liu, Y. Guang, K. Yue, J. Feng, R. Lake, G. Yu, and X. Han, “Skyrmion-based programmable logic device with complete boolean logic functions,” *Physical Review Applied* **15**, 064004 (2021).